ORIGINAL PAPER

Contact Mechanics and Friction on Dry and Wet Human Skin

B. N. J. Persson · A. Kovalev · S. N. Gorb

Abstract The surface topography of the human wrist skin is studied using an optical method and the surface roughness power spectrum is obtained. The Persson contact mechanics theory is used to calculate the contact area for different magnifications, for both dry and wet condition of the skin. For dry skin, plastic yielding becomes important and will determine the area of contact observed at the highest magnification. The measured friction coefficient [M.J. Adams et al., Tribol Lett 26:239, 2007] on both dry and wet skin can be explained assuming that a frictional shear stress $\sigma_f \approx 15$ MPa acts in the area of real contact during sliding. This frictional shear stress is typical for sliding on polymer surfaces, and for thin (nanometer) confined fluid films. The big increase in the friction, which has been observed for glass sliding on wet skin as the skin dries up, can be explained as resulting from the increase in the contact area arising from the attraction of capillary bridges. This effect is predicted to operate as long as the water layer is thinner than ~ 14 μm, which is in good agreement with the time period (of order 100 s) over which the enhanced friction is observed (it takes about 100 s for ~ 14 μm water to evaporate at 50% relative humidity and at room temperature). We calculate the dependency of the sliding friction coefficient on the sliding speed on lubricated surfaces (Stribeck curve). We show that sliding of a sphere and of a cylinder gives very similar results if the radius and load on the sphere and cylinder are appropriately related. When applied to skin the calculated Stribeck curve is in good agreement with experiment, except that the curve is shifted by one velocity-decade to higher velocities than observed experimentally. We explain this by the role of the skin and underlying tissues viscoelasticity on the contact mechanics.

1 Introduction

The tribology of the human skin is a fascinating but very complex topic. This is partly due to the layered nature of skin, to its complex viscoelastic nature, and to its great sensitivity to the humidity. Thus, it is known that the effective elastic modulus of the skin top-layer (the $d \approx 20$ μm thick *stratum corneum*) may change by a factor of $\sim 100-1000$ as the humidity increases from zero to 100% relative humidity (see Ref. [1] and references therein). At low humidity the stratum corneum has an elastic modulus similar to rubber in the glassy region (with a Young's modulus $E \approx 1-3$ GPa), while in the wet state it behaves as rubber in the rubbery region with the Young's modulus of order $E \approx 5-10$ MPa (see Refs. [1, 2]). However, if the skin, e.g., on the inner forearm, is probed by a macroscopic indentor, e.g., a ball with the diameter of order ~ 1 cm, the (macroscopic) contact mechanics is well described using the Hertz contact model with an effective elastic modulus $10-40$ kPa. This reflect the softness of the tissue layers below the skin layer. Thus, the contact mechanics between the indentor and the skin can only be described using a layer-model with a thin elastically stiff layer on the top of a soft bulk.

B. N. J. Persson (✉)
IFF, FZ-Jülich, 52425 Jülich, Germany
e-mail: b.persson@fz-juelich.de

A. Kovalev · S. N. Gorb
Department of Functional Morphology and Biomechanics,
Zoological Institute at the University of Kiel, Am Botanischen
Garten 1-9, 24098 Kiel, Germany

Due to its importance for living objects, it is likely that the skin has been highly optimized during million of years of evolution. This probably also reflect its tribology properties and it is likely that many of its mechanical and structural properties reflect this fact. Thus, the pattern of channels on the skin surface on the hands may facility the squeeze-out of fluids (similar to the tread pattern on tires) and may increase the friction and grip between a fluid-contaminated object and the human hand [3]. Similarly, the strong reduction in the elastic modulus of the stratum corneum in humid condition result in a large increase in the contact area and the friction during sweating, which again may increase the friction or grip between the hand and an object, which may be particularly important in emergency situations.

A large number of studies have been performed on the tribology of the human skin [4]. This is partly because of its great importance in medicine and cosmetics, and partly because of curiosity. The present understanding has been summarized in a beautiful article by Adams et al [1], and we will compare some of our theoretical predictions below to the results presented by Adams et al. We emphasize that the tribology of the skin is a very complex topic. Nevertheless, we believe that the picture presented in our article correctly describe the properties of human skin, and that the calculated results are at least of semi-quantitative accuracy.

This article is organized as follows: In Sect. 2, we present optical surface topography data of the skin, and in Sect. 3 we calculate the surface roughness power spectra which is used in the contact mechanics calculations. In Sect. 4, we calculate the contact area between skin and a hard flat surface and derive the magnitude of the stress which must exist in the area of real contact during sliding on dry and wet skin. In Sect. 5, we discuss the role of capillary bridges on the contact mechanics and show that the large peak in the friction force observed during drying of wet skin can be explained by the increase in the contact area resulting from the capillary attraction (for hydrophilic interfaces). In Sect. 6, we discuss mixed lubrication. We first show that by appropriate choice of the radius and load, the lubricated friction dynamics is very similar for spherical and cylindrical sliding objects. Next, we calculate the Stribeck curve for skin and compare it to the measured results of Adams et al. Sect. 7 contains the summary.

2 Experimental

Wrist skin topography was analyzed in dry and wet states. The skin was first washed with ethanol, then wiped and dried for 2 min. To transfer the skin in a wet state, a wet napkin was placed on the skin surface for 10 min. Before
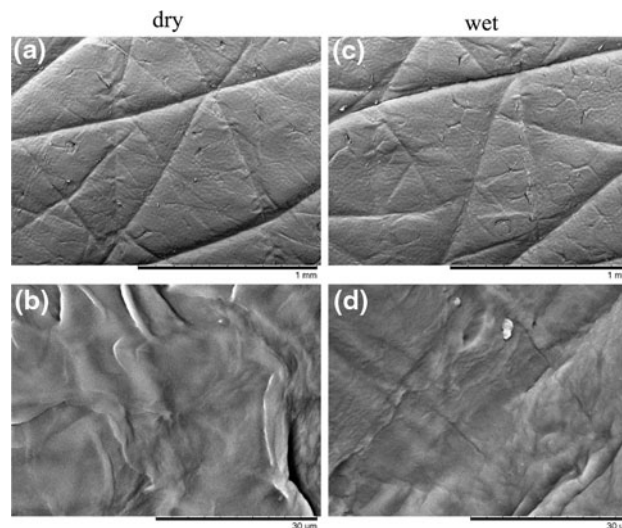
Fig. 1 SEM picture of dry (**a**, **b**) and wet (**c**, **d**) human wrist skin taken at low (**a**, **c**) and high (**b**, **d**) magnification

further manipulations the skin was wiped and dried for 2 min. A two-component dental wax (President light body, Coltene, Switzerland) was used to prepare the negative casts of the skin in dry and wet state. The negative casts were further filled out by Spurrs low-viscosity resin and polymerized overnight at 70C. The images of positive epoxy casts coated with gold-palladium (4 nm) were obtained using a Hitachi TM3000 tabletop electron microscope (Hitachi High-Technologies Corp., Tokyo, Japan) at an accelerating voltage of 3 kV (see Fig. 1). 3D-surface profiles of negative casts were acquired using a white-light interferometer NewView 6k (Zygo, Middlefield, CT, USA) with 5x and 50x magnifications (see Fig. 2). Contact angles of water on the skin were measured 5 times at different locations for each skins state using a contact angle measurement device OCA20 (Dataphysics
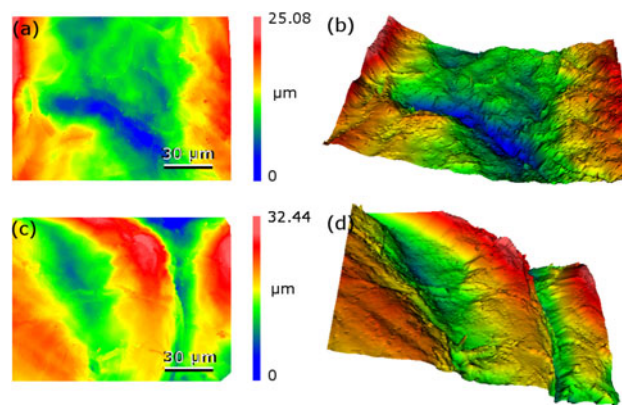
Fig. 2 White-light-interferometer pictures of dry (**a**, **b**) and wet (**c**, **d**) human wrist skin. **a**, **c** 2D view of the surface with the color coded heights. **b**, **d** 3D views of the same surface as in **a**, **c** with color coded heights (Color figure online)

Instruments, Filderstadt, Germany). According to our measurements the advancing water contact angle on human wrist skin is $112.9 \pm 1°$ on dry skin and $121.4 \pm 1.6°$ on wet skin. The larger contact angle on wet skin could reflect either a change in the skin surface chemistry, or more likely may be due to the increase in the surface roughness of wet skin. The receding contact angle was not measured but will be smaller than the advancing contact angle. There are different values for the water- skin contact angle published in the literature in the range $80-110°$.

## 3 Surface Roughness Power Spectrum of Skin

From the measured height profile $z = h(\mathbf{x})$ (where, $\mathbf{x} = (x, y)$ is the in-plane coordinate) we calculate the surface roughness power spectrum defined by [5, 6]

$$C(\mathbf{q}) = \frac{1}{(2\pi)^2} \int d^2x \langle h(\mathbf{x})h(\mathbf{0})\rangle e^{-i\mathbf{q}\cdot\mathbf{x}} \quad (1)$$

where $\langle ..\rangle$ stands for ensemble average and where $\mathbf{q} = (q_x, q_y)$ is a two-dimensional (2D) wavevector of a particular cosines-surface roughness component with wavelength $\lambda = 2\pi/q$ and orientation (in the xy-plane) determined by the direction of $\mathbf{q}$. For surfaces with roughness with isotropic statistical properties, $C(\mathbf{q})$ depends only on $q = |\mathbf{q}|$.

Figure 3 shows the power spectra as a function of the wave vector ($\log_{10}$–$\log_{10}$ scale). The red and green lines are from dry skin (red from our laboratory and green from the surface topography presented in Fig. 10 in Ref. [1]). The blue lines are for wet skin.

In Fig. 4, we show the power spectra on a larger wave-vector range. The red and blue lines are from Fig. 3. The lower green line is the power spectrum used in the calculations presented below (e.g., in Fig. 8), and corresponds to a
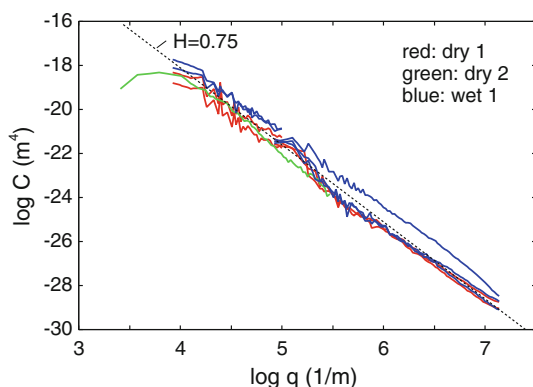
Fig. 3 The power spectra as a function of the wave vector ($\log_{10}$–$\log_{10}$ scale). The *red* and *green* lines are from dry skin (*red* from our laboratory and *green* from the surface topography presented in Fig. 10 in Ref. [1]). The *blue lines* are for wet skin (Color figure online)
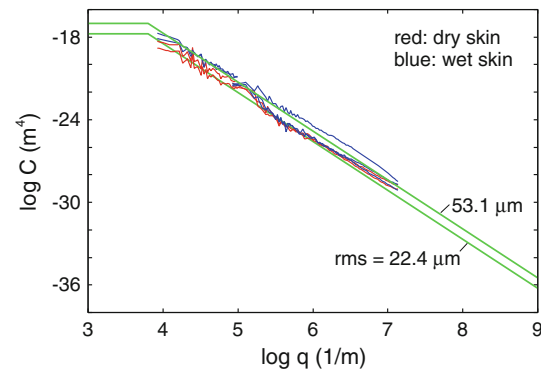

Fig. 4 The power spectra as a function of the wave vector ($\log_{10}$–$\log_{10}$ scale). The *blue lines* are for wet skin and the *red* for dry skin. The *green lines* are fit to the measured data. The lower *green line* is the power spectra used in the calculations and correspond to a surface with the surface area $A_{tot} = 2.7 A_0$ and rms slope 2.8 (Color figure online)

self-affine fractal surface with the fractal dimension $D_f = 3 - H = 2.22$, the rms roughness 22.4 μm, the total surface area $A_{tot} = 2.7 A_0$ (where A_0 is the nominal or projected surface area) and the rms slope 2.8. The smallest surface roughness wavevector $q_0 = 10^3$ m^{-1} and the largest (cut-off) wavevector $q_1 = 10^9$ m^{-1}. The upper green line has the same fractal properties as the lower green line, but correspond to a rms roughness about twice as large as for the lower green line, and is shown to indicate the variability in the power spectrum between different measurements and surfaces.

4 Contact Mechanics of Dry and Wet Skin

Figure 5 shows the model of the skin used in all the calculations presented below. The bulk elastic modulus $E_1 = 20$ kPa and Poisson ratio $\nu_1 = 0.5$. The top-layer (stratum corneum) is $d = 20$ μm thick and has the Young's modulus $E_0 = 7$ MPa in the wet state and $E_0 = 1$ GPa in the dry state and the Poisson ratio $\nu_0 = 0.5$. For the dry skin, the contact pressures becomes so high that plastic deformations of the skin must be taken into account. We use the plastic yield stress (or penetration hardness) $\sigma_Y = 50$ MPa in the calculations presented below. The yield stress of most polymers are of order ~ 100 MPa, but experiment (see Ref. [7]) indicates that the yield stress of human skin may be $\sigma_Y \approx 50$ MPa .This is about 5% of the Youngs modulus, which is typical for many materials, e.g., similar to what is observed for dry cellulose fibers. In fact cellulose fibers exhibit very similar elastoplastic properties as the stratum corneum e.g., both can absorb a lot of water and swell by ~ 100 %, and both have elastic moduli in the order of 10 MPa in the wet state and of order 1 GPa in the dry state [8]. And the origin for the swelling (and elastic softening) in water seems to be the
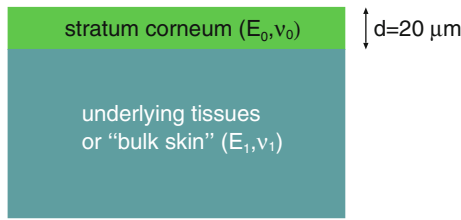
Fig. 5 The model of the skin used in the calculations. The bulk elastic modulus $E_1 = 20$ kPa and Poisson ratio $v_1 = 0.5$. The top-layer (stratum corneum) is $d = 20$ μm thick and has the Young's modulus $E_0 = 7$ MPa in the wet state and $E_0 = 1$ GPa in the dry state and the Poisson ratio $v_0 = 0.5$. For dry skin, we assume the penetration hardness $\sigma_Y = 50$ MPa

same for the skin and cellulose fibers, namely the break-up of hydrogen bonds (by the water) in the wet state. The elastoplastic parameters given above are in accordance with experimental measurements [1, 7], although there are relative large variations in these parameters between different measurements.

We have used the Persson contact mechanics theory to analyze the contact between skin and a flat hard counter-surface. The surface area observed when the interface is studied at the magnification ζ, where the surface roughness with wavevector $q > q_0 \zeta$ cannot be detected, is given by [5, 9]

$$\frac{A(\zeta)}{A_0} = \text{erf}\left(\frac{1}{2\sqrt{G}}\right) \tag{2}$$

where $\text{erf}(x)$ is the error function and

$$G(\zeta) = \pi \int_{q_0}^{\zeta q_0} dq\, q |\sigma_0 M_{zz}(q)|^{-2} C(q) \tag{3}$$

where $\sigma_0 = p_0$ is the applied stress or pressure. The linear response function M_{zz} relate (in wavevector space) the surface displacement normal to the surface to the stress acting normal to the surface: $M_{zz}(q) = u_z(q)/\sigma_z(q)$. For a layered material of the type shown in Fig. 5 it is given by $M_{zz} = -2\, S(q)/(qE_0^*)$ [where $E_0^* = E_0/(1 - v_0^2)$] where [10–12]

$$S(q) = \frac{1 + 4mqde^{-2qd} - mne^{-4qd}}{1 - (m + n + 4mq^2d^2)e^{-2qd} + mne^{-4qd}} \tag{4}$$

where

$$m = \frac{G_0/G_1 - 1}{G_0/G_1 + 3 - 4v_0}$$

$$n = 1 - \frac{4(1 - v_0)}{1 + (G_0/G_1)(3 - 4v_1)}$$

where $G_0 = E_0/2(1 + v_0)$ is the shear modulus of solid 0 and similar for solid 1.

Figure 6 shows the area of contact (in units of the nominal contact area A_0) as a function of the magnification ζ (lower

scale) or the wavevector q (upper scale) of the highest roughness components included in the calculation ($\log_{10}-\log_{10}$ scale). We note that the area of (apparent) contact depends on the magnification or resolution of the instrument used to study the contact and only an instrument with atomic resolution will detect the area of real (or atomic) contact. An optical instrument, for example, with resolution limited by the wavelength of light, would detect (for transparent materials) a larger contact area than an instrument with atomic resolution because regions at the interface where the interfacial separation is smaller than (some fraction of) the wavelength of light would appear as contact in the optical picture. In all the calculations presented below we have assumed the squeezing pressure $F_N/A_0 = p_0 = 6.83$ kPa, which is the average nominal contact pressure in the experiments reported on in Fig. 7. The blue curve is for wet skin and red curve for dry skin. At the highest magnification the relative contact area is $A/A_0 = 6.59 \times 10^{-4}$ for wet skin and 1.37×10^{-4} for dry skin. For dry skin complete plastic yielding occur in all contact regions so that $A/A_0 = \sigma_N/\sigma_Y = 1.37 \times 10^{-4}$. Note that plastic deformation starts already at $q \approx 10^5$ m^{-1} corresponding to a wavelength $\lambda = 2\pi/q \approx 60$ μm. The frictional shear stress necessary to explain the observed friction coefficients (which are $\mu \approx 0.3$ on dry skin and ≈ 1.4 on wet skin) are ≈ 15 MPa for both dry and wet surfaces. This is very similar to the frictional shear stress for sliding on polymers [13], or for many thin (~ 1 nm) confined fluid layers between hard surfaces [14].

The area of real contact obtained in the present study is much smaller than assumed in Ref. [1] where for wet skin the authors assumed (without proof) $A/A_0 \approx 1$. However, the value we obtained is a direct result of the assumed
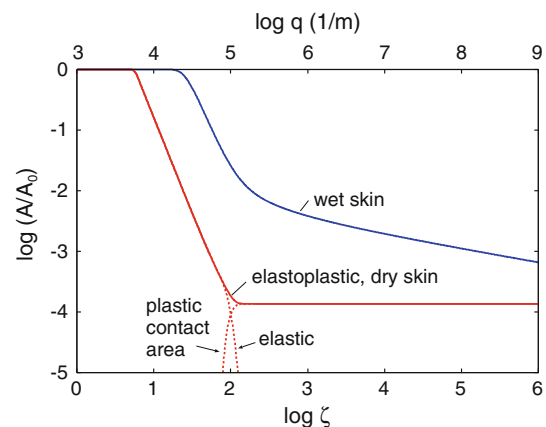
Fig. 6 The area of contact (in units of the nominal contact area A_0) as a function of the magnification ζ (*lower scale*) or the wavevector q (*upper scale*) of the highest roughness components included in the calculation ($\log_{10}-\log_{10}$ scale). The squeezing pressure $F_N/A_0 = p_0 = 6.83$ kPa. The *blue curve* is for wet skin and and the *red curve* for dry skin. The skin model shown in Fig. 5 is used in the calculations (Color figure online)
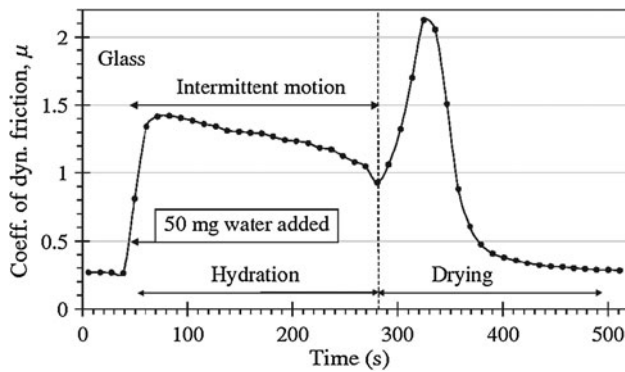
Fig. 7 The friction coefficient of skin for a glass ball ($R = 0.8$ cm) at a sliding velocity 0.8 cm/s and normal load 0.5 N during wetting/drying. Adopted from Ref. [1] with the permission of the authors

elastoplastic properties and the measured surface roughness of the stratum corneum. We also note that although the surface stress acting on the stratum corneum for dry skin is predicted to be very high (of order 50 MPa), it correspond to relative small strain values, and the stresses acting on the living cells below the stratum corneum, due to their low effective elastic modulus, will be much smaller and is unlikely to damage the cells.

5 Capillary Adhesion

The measured friction coefficient when a small glass ball (radius $R = 0.8$ cm) is sliding on wet skin is shown in Fig. 7. The sliding velocity 0.8 cm/s and the normal load 0.5 N. At $t \approx 30$ s a $\Delta V = 50 \times 10^{-9}$ m^3 water droplet is added to the sliding track. This correspond to an average water film thickness on the track of order $d \approx \Delta V/LD \approx 90\,\mu$m, where $L \approx 8$ cm is the stroke length and $D \approx 0.8$ cm the width of the (nominal) Hertz's contact region. A uniform water film of thickness $\Delta d = 90\,\mu$m will at room temperature and 50% relative humidity evaporate in about 500 s (here we have used the evaporate rate $\dot{d} \approx 1.7 \times 10^{-7}$ m/s, see below). This is exactly the time period necessary for the friction to return to the dry state value (see Fig. 7).

We will now show that the sharp peak in the coefficient of friction which is observed as the water evaporate, see Fig. 7, can be explained as resulting from the increase in the area of real contact arising from the attractive force from capillary bridges. We can take into account capillary bridges in an approximate way as described in detail in Ref. [15]. That is, we put water at the interface between the skin and the glass surface in all regions where the separation is less than the Kelvin length:

$$d_K = -r_K(\cos\theta_1 + \cos\theta_2) \tag{5}$$

In the fluid regions the (negative) Laplace pressure acts

$$p_K \approx -\gamma/r_K \tag{6}$$

where γ is the surface tension of water. If ΔA is the surface area occupied by the capillary bridges then the attractive force

$$F_a = |p_K|\Delta A \tag{7}$$

We define $p_a = F_a/A_0$ and we calculate the contact area and the distribution of interfacial separations using the Persson contact mechanics model with the external pressure p_0 replaced by the total pressure $p = p_0 + p_a$. In this mean-field approximation, the force from the non-uniform distribution of capillary bridges is replaced by a uniform pressure or stress p_a. Note that to calculate ΔA we need to know the pressure $p = p_0 + p_a$ but since p_a depends on ΔA [see (7)] we have an implicit equation for ΔA or p_a which can be solved, e.g., by iteration.
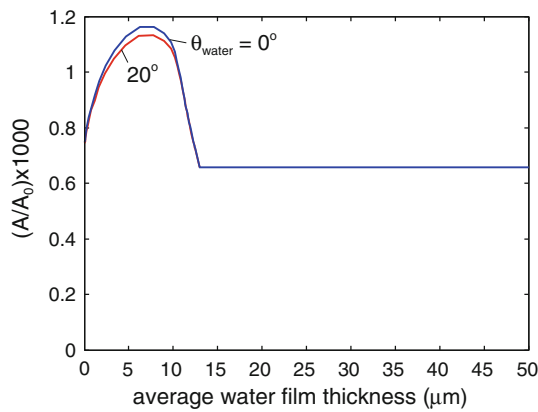
Figure 8 shows the area of real contact (in units of the nominal contact area A_0) (times a factor 1000) as a function of the average water film thickness d. For $d > 14$ μm the water cover all the interface (flooded condition). We have assumed the (receding) contact angle $\theta = 20°$ (red curve) and $0°$ (blue curve) for water on glass and $80°$ for water on skin. The increase in the contact area for the average water film thickness between 0 and ≈ 14 μm is due to the formation of capillary bridges. Since the contact area is small compared to the nominal contact area, the area of real contact is proportional to the effective squeezing force $p_0 + p_a$. Thus at the point where the contact area is maximal, $p_a \approx 0.7 p_0$, i.e., the attractive capillary pressure is of similar magnitude as the (nominally) applied pressure $p_0 \approx 7$ kPa. We will now show that the width (in seconds) of the friction peak observed in Fig. 7 correspond to a change in the average water film thickness (due to evaporation) of ≈ 14 μm, in beautiful agreement with the width of our predicted friction peak.

The water evaporation rate $\dot{d}$ (change per unit time of the fluid film thickness d) is given by the empirical formula [1]

$$\dot{d} \approx -(p_w - p_a) \times (a + bv)/Y \tag{8}$$

where p_w is the water saturation vapor pressure at the water (surface) temperature, p_a is the water vapor pressure in the air (which is the product of the relative humidity and the saturation water pressure at the air temperature and air pressure), and v the velocity of the air (some distance from the water surface) over the water surface. Y is the latent heat of evaporation (for water $Y \approx 2,272$ kJ/kg) and where $a = 8.9 \times 10^{-5}$ m^4/(kg s) and $b = 7.8 \times 10^{-5}$ m^3/kg. If the

---

[1] See the ASHRAE Handbooks published by the technical organization American Society of Heating, Refrigerating and Air-Conditioning Engineers, Inc. (ASHRAE). This Handbook is considered the practical repository of knowledge on the various topics that form the field of heating, ventilation, air-conditioning, and refrigeration.

Fig. 8 The area of real contact (in units of the nominal contact area A_0) (times a factor 1000) as a function of the average water film thickness d. For $d > 14$ μm the water cover all the interface (flooded condition). The squeezing pressure $F_N/A_0 = p_0 = 6.83$ kPa. In the calculations, we have used the skin model shown in Fig. 5 and assumed the contact angle $\theta = 20°$ (*red curve*) and 0° (*blue curve*) for water on glass and 80° for water on skin (Color figure online)

water on the skin has a temperature close to the body temperature, say $T = 35°$ C, then $p_w = 5.6$ kPa. The experiments was performed at room temperature ($T = 20°$ C) and relative humidity 50% giving $p_a = 0.5 \times 2.3$ kPa = 1.15 kPa. Hence, since $v \ll 1$ m/s, we get $\dot{d} \approx 1.7 \times 10^{-7}$ m/s. Thus it takes $\Delta t = \Delta d/\dot{d} \approx 76$ s for the water film thickness to decrease by $\Delta d \approx 14$ μm, which according to the theory is the film thickness range over which the capillary attraction between the surfaces is effective. This is in beautiful agreement with the experimental data (see Fig. 7).

We have assumed that the thermodynamic water-skin contact angle is $\theta_1 \approx 80°$, and the water-glass contact angle $\theta_2 \approx 20°$. Thus, $\cos\theta_1 + \cos\theta_2 \approx 1 > 0$ so that the interface is hydrophilic and attractive capillary bridges can form. In a second friction experiment, Adams et al [1] used a polypropylene sphere and in this case no increase in the friction was observed during drying. This is consistent with the fact that the water-polypropylene contact angle $\theta_2 \approx 102°$ so that $\cos\theta_1 + \cos\theta_2 \approx -0.04 < 0$ so the interface may be slightly hydrophobic resulting in a negligible interaction between the walls during drying. For more strongly hydrophobic interfaces, e.g., skin in contact with Teflon in water, a dewetting transition may occur resulting in dry contact area and an effective attraction between the skin and the countersurface [16].

A friction peak has also been observed for wiper blades sliding on a wet glass surface during drying [17]. This system has similar elastic properties as for the wet skin, but the rubber surface is smoother and the nominal contact pressure much higher (of order MPa). Thus, the average surface separation is much smaller for skin, and the water film is much thinner. This result in much stronger capillary

forces than observed for skin and gives a relative large increase in the contact area in spite of the large nominal squeezing pressure. As a result of the thinner fluid film, the enhanced friction only prevail for ~ 5 s during drying.

Another experiment [18] under conditions similar to that of the skin friction was performed with a rubber block squeezed by a low nominal pressure (of order 10 kPa) against a steel surface. During sliding at ~ 0.1 m/s it was observed that if a small oil drop was added at the sliding interface the friction coefficient increased from ~ 1 to ~ 3, when the rubber block passed over the region covered by the oil film. This can be naturally explained by the additional attraction from the oil capillary bridges between the rubber and the steel track.

Figure 9 shows the area of contact (times 1000) (blue line) and the wet area (black line) (both in units of the nominal contact area A_0) as a function of the average water film thickness. Figure 10 shows the average interfacial separation $\bar{u}$, and the average interfacial separation in the wet area, as a function of the average water film thickness. Note that the capillary adhesion force makes the surfaces approach each other from $\bar{u} \approx 13$ μm without the capillary adhesion (e.g., for flooded surface) to ≈ 10 μm for the average water film thickness $\approx 6-9$ μm, where the capillary adhesion is maximal.

In this section, we studied the influence of relative thick water films (average film thickness of order $\sim 1-10$ μm) on the skin-glass contact mechanics. Such film thickness prevails, for example, during drying of an originally flooded contact. Similar film thickness may prevails during sweating. In Appendix A, we consider instead skin in equilibrium with humid air as a function of the air relative humidity. For most humidity this implies water film thickness of order a few nanometers or less.
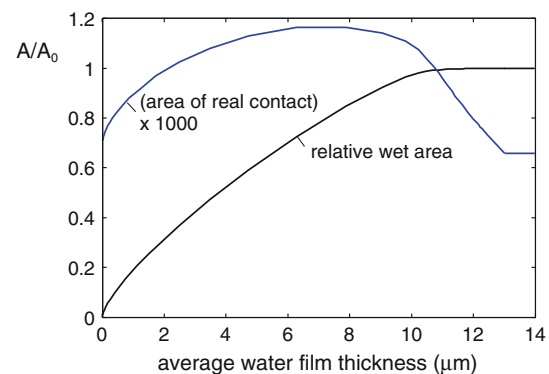
Fig. 9 The area of contact (times 1000) (*blue line*) and the wet area (*black line*) (both in units of the nominal contact area A_0) as a function of the average water film thickness. The squeezing pressure $F_N/A_0 = p_0 = 6.83$ kPa. For the calculations, we have used the skin model shown in Fig. 5 and the water-glass contact angle 0°
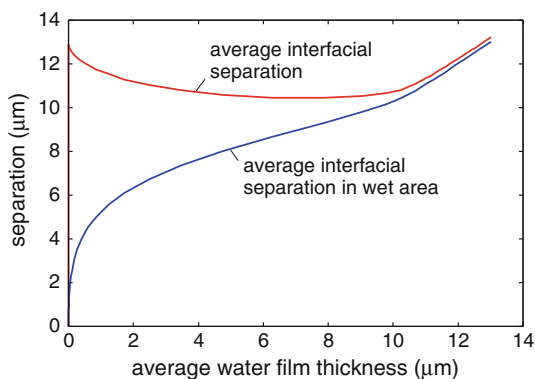
Fig. 10 The average interfacial separation and the average interfacial separation in the wet area, as a function of the average water film thickness. The squeezing pressure $F_N/A_0 = p_0 = 6.83$ kPa. In the calculations we have used the skin model shown in Fig. 5 and the water-glass contact angle 0°

It was previously shown that humidity influences adhesion of some biological materials, such as attachment setae of geckos and spiders [19, 20]. Huber et al. [20] first showed that adhesion of a single gecko spatula on different substrates increases linearly with increasing environmental humidity. Later, an increase in the attachment ability of the gecko together with increasing humidity was demonstrated for living geckos [21] and spiders [22]. In connection with skin, an essentially linear relationship between skin hydration and friction was found for forearm skin [23–25] and for finger skin [26, 27].

The influence of capillary bridges is also of importance in a huge number of other applications, e.g., for binding of the cellulose fibers in paper, and also for adhesion of the tree frog and insects to surfaces. It is the reason for why we (often) wet the finger before turning a page in a book or news paper.

6 Mixed Lubrication and Stribeck Curve

In this section, we first show how one can (approximately) map the sliding dynamics of a sphere on a lubricated substrate on a problem of a cylinder sliding on the same substrate. This is not only useful from a computational point of view but also interesting from a conceptional point of view. This type of mapping should be even more accurate for a Hertz elliptic contact with the sliding direction orthogonal to the major elliptic axis and we consider this case in Appendix B. We then apply this to the case of a glass ball sliding on lubricated skin, and compare the results to the measurements of Adams et al [1].

6.1 Sliding Sphere and Cylinder

In the applications below, we are interested in a glass ball sliding on lubricated (with silicon oil) human skin. One of us

has studied the sliding of balls and cylinders on lubricated, elastic substrates, in several earlier publications [28–30]. However, the most complete theory [29], which takes into account the fluid pressure and shear stress flow factors, and the frictional shear stress factors (which is a formally exact way of including the influence of the surface roughness on the fluid dynamics) has only been implemented in the numerical code for sliding cylinders. Here, we first show that for trivial fluid flow and shear stress factors (see Ref. [29]) one can to a very good approximation obtain the friction force acting on a sphere from the result for a cylinder, assuming that the radius of the cylinder and the load on the cylinder is chosen so that (a) the average Hertz contact pressure is the same, and (b) so that the condition $r_0 = w\sqrt{(2/3)}$ is satisfied, where w is the width of the Hertz infinite rectangular contact strip for the cylinder, and r_0 the radius of the circular contact region for the sphere. The latter condition guaranty the same fluid squeeze-out time for an infinite rectangular sheet (width w) as for a circular disk (radius r_0) (both rigid and with identical applied squeezing pressures).

Let R_s be the radius of the sphere, and R_c of the cylinder, and F_N the load on the sphere, and f_N the load per unit length one the cylinder. The average contact pressure and the radius of the circular contact region for a sphere squeezed against a flat surface is [31]:

$$\bar{p}_s = \frac{2}{3\pi}\left(\frac{6F_N E^{*2}}{R_s^2}\right)^{1/3}, \quad r_0 = \left(\frac{3F_N R_s}{4E^*}\right)^{1/3}$$

and for the cylinder case:

$$\bar{p}_c = \frac{\pi}{4}\left(\frac{f_N E^*}{\pi R_c}\right)^{1/2}, \quad w = 4\left(\frac{f_N R_c}{\pi E^*}\right)^{1/2}$$

The conditions $\bar{p}_s = \bar{p}_c$ and $r_0 = w(2/3)^{1/2}$ gives

$$R_c = CR_s, \quad f_N = C'\left(\frac{E^* F_N^2}{R_s}\right)^{1/3} \tag{9}$$

where

$$C = \frac{\pi^2}{32}\left(\frac{3}{2}\right)^{3/2} \approx 0.567, \quad C' = \pi^{-1}6^{1/6} \approx 0.429$$

To illustrate the accuracy of the approach described above, in Fig. 11 we show the Stribeck curves for a sphere and a cylinder sliding on lubricated rough surfaces. The sphere-case is from Fig. 25 in Ref. [28], while the cylinder case is with the radius and load given by (9). The sphere has the radius $R = 1$ cm and the load $F_N = 1.3$ N. The effective elastic modulus $E^* = 1.6$ MPa. This figure, and other similar calculations, show that the mixed lubrication problem for a sphere can be approximately treated using the (simpler) cylinder geometry if the radius R_c of the cylinder,
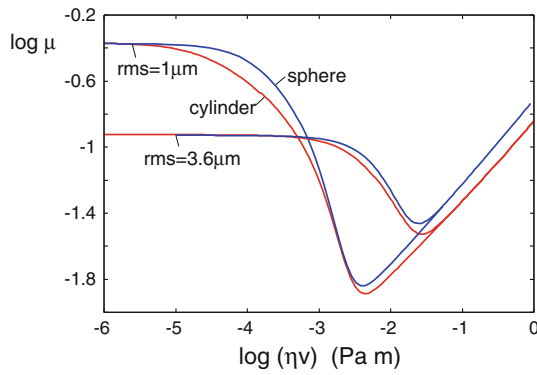
Fig. 11 Stribeck curves for sphere and cylinder sliding on lubricated rough surfaces. The sphere case is from Fig. 25 in Ref. [28] while the cylinder case is discussed in the text. The sphere has the radius $R = 1$ cm and the load $F_N = 1.3$ N. The effective elastic modulus $E^* = 1.6$ MPa. The mixed lubrication problem for a sphere can be approximately treated using the (simpler) cylinder geometry if the radius R_s of the sphere, and R_c of the cylinder, and load F_N on the sphere, and the load per unit length f_N one the cylinder, are chosen so that the average Hertz contact pressure is the same, and so that the condition $r_0 = w\sqrt{(2/3)}$ is satisfied, where w is the width of the Hertz rectangular contact strip for the cylinder and r_0 the radius of the circular Hertz contact region for the sphere. The latter condition guaranty the same fluid squeeze-out time for an infinite rectangular sheet (width w) as for a circular disk (radius r_0) (both rigid and with applied squeezing forces related as described above)

and the load per unit length f_N one the cylinder, are chosen according to (9). Note that in the hydrodynamic region the slope of the two friction curves for the cylinder and the sphere in Fig. 11 are slightly different (≈ 0.47 and ≈ 0.50 for the cylinder and the sphere, respectively) but the numerical difference is not large in the studied velocity range.

6.2 Stribeck Curve for Skin

Figure 12 shows the measured [1] Stribeck curve based on the sliding of a glass ball ($R = 0.8$ cm) on skin at an applied load of $F_N = 0.2$ N, with sliding velocities in the range 0.1–5 cm/s for silicone fluids of viscosity between $\eta_0 = 0.0008$ Pa s to 58.8 Pa s.
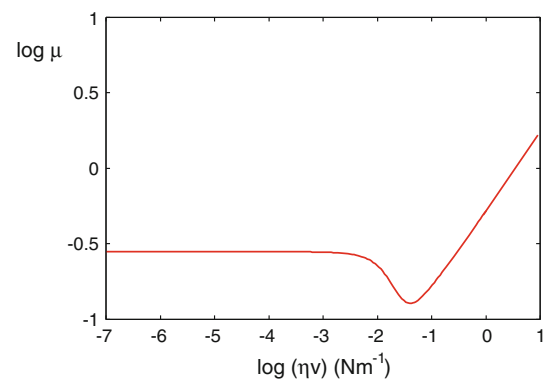
Figure 13 shows the calculated Stribeck curve for a glass ball ($R = 0.8$ cm) sliding on skin at an applied load of $F_N = 0.2$ N. In the calculation we have used the mapping of the sphere problem on the cylinder problem discussed above. The results has been obtained including the pressure and shear flow factors and the frictional shear stress factors as described in Ref. [29] (see also Appendix C). The theory curve is similar to the measured results and the minimum friction coefficient is nearly the same as found experimentally. However, the theoretical friction curve is shifted by a factor ~ 20 to higher velocities than observed. (The strait line in the hydrodynamic region in Fig. 12 is based on an
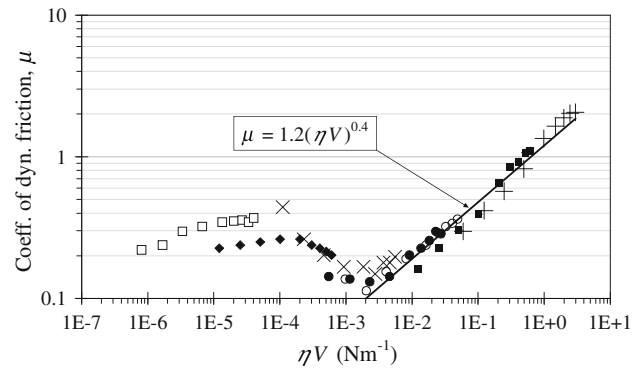
Fig. 12 A Stribeck curve based on the sliding of a glass ball ($R = 0.8$ cm) on skin at an applied load of $F_N = 0.2$ N, with sliding velocities in the range 0.1–5 cm/s for silicone fluids of viscosity between 0.0008 and 58.8 Pa s. Adopted from Ref. [1] with the permission of the authors

approximate treatment of the elastohydrodynamic problem suggested by Johnsson, but the fact that this curve agrees better with the experiment in the hydrodynamic region than the full theory is just a coincidence.) In Appendix C, we show that using trivial frictional shear stress and fluid flow factors gives nearly the same result as the full calculation presented above, indicating that the small inaccuracy in the flow factors cannot explain the difference between theory and experiment. Similarly, shear thinning of the silicon oil [32–34] has in the present case not a big effect on the theory results (see Appendix C). We attribute this to the small nominal contact pressure and large average surface separation which prevail in the skin friction experiments.

We believe the reason for the velocity shift is related to the viscoelastic nature of the skin and underlying tissues. This is illustrated in Fig. 14 which shows a hard sphere (or cylinder) sliding on a viscoelastic substrate (e.g., skin). Note that due to the viscoelasticity, the substrate

Fig. 13 The theoretically predicted Stribeck curve for a glass ball ($R = 0.8$ cm) sliding on skin at an applied load of $F_N = 0.2$ N. We have used the frictional shear stress in the area of real contact $\sigma_f = 15$ MPa as obtained earlier for dry skin (see Sect. 4)
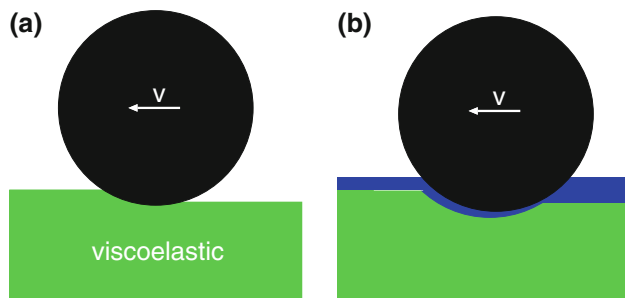
Fig. 14 A hard sphere (or cylinder) sliding on a viscoelastic substrate (e.g., skin). **a** Due to the viscoelasticity of the substrate, the deformations are asymmetric around lowest point of the sphere (the substrate is lowered on the exit side of sliding due to the finite recovery time of the viscoelastic material). **b** When the ball slides on the substrate in a viscous fluid, the viscoelastic deformations of the substrate will modify the interfacial separation in such a way as to increase the separation on the exit side of the sliding junction, which will lower the velocity necessary for direct asperity contact between the solids (since asperity contact occurs first on the exit side of the sliding junction)

deformations are asymmetric around lowest point of the sphere (the substrate is lowered on the exit side of sliding due to the finite recovery time of the viscoelastic material) (see Fig. 14a). When the ball slides on the substrate in a viscous fluid (Fig. 14b), the viscoelastic deformations of the substrate will modify the interfacial separation in such a way as to increase the separation on the exit side of the sliding junction, which will lower the velocity necessary for direct asperity contact between the solids (since the separation between the solids for elastic solids is smallest on the exit side of the sliding junction). Thus, the hydrodynamic region will extend to lower sliding velocities, in agreement with the observations. In order for this effect to be large, the loss tangent $\tan\delta$ must be large enough for the relevant frequencies which are of order $v/D \sim 1 \ \mathrm{s}^{-1}$, where v is the sliding velocity (of order mm/s) and D the diameter of the Hertz contact region (which is of order a few mm). We note that indentation (loading–unloading) experiments (velocity 2.5 mm/s, indentation depth 5 mm) with glass sphere against the human inner forearm gives a hysteresis energy loss of order 25 % of the elastic input energy, and a temporary set of about 0.5 mm which is recovered only at longer time scales [35]. This support the explanation presented above for the shift of the Stribeck curve to lower sliding speeds than predicted assuming a perfect elastic substrate.

Skin viscoelasticity will also give a direct contribution to the rolling or sliding friction [36], but the study in Ref. [1] indicate that this contribution to the friction coefficient is rather small, of order 0.05 or so. However, during sliding on hard rough substrates the pulsating viscoelastic deformations of the rubber induced by the substrate asperities may give an important contribution to the friction just as
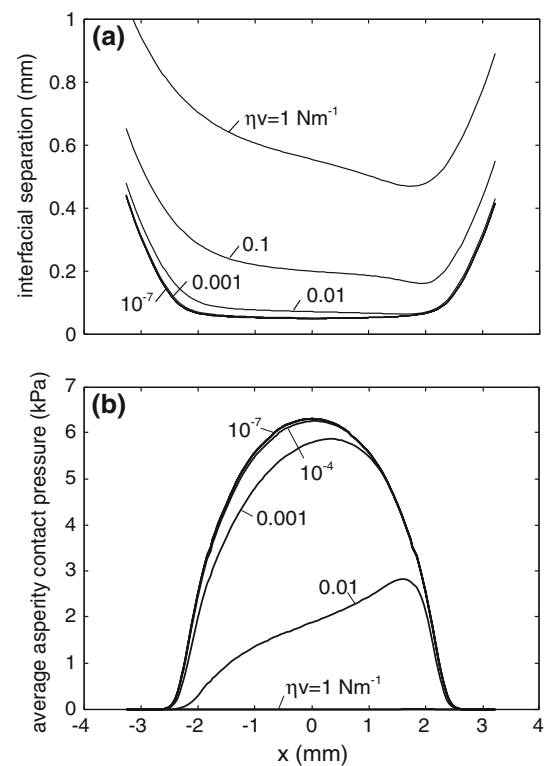
Fig. 15 The average interfacial separation $\bar{u}$ (**a**) and the (average) asperity contact pressure (**b**), as a function of the position x for the sliding velocities $\eta v = 10^{-7}, 10^{-6}, \ldots, 1, 10 \ \mathrm{Nm}^{-1}$. Note that the separation is smallest on the exit side of the sliding junction where the asperity contact will be strongest

for rubber-like materials [11]. However, this contribution cannot be calculated until the frequency-dependent viscoelastic modulus of the skin is better understood.

Figure 15 shows the (calculated) average interfacial separation $\bar{u}$ and the (average) asperity contact pressure, as a function of the position x for the sliding velocities $\eta v = 10^{-7}, 10^{-6}, \ldots, 1, 10 \ \mathrm{Nm}^{-1}$. Note that the separation is smallest on the exit side of the sliding junction where the asperity contact will be strongest.

7 Discussion

In the study in this article, we have focused on experimental results obtained for the skin on the inner forearm. However, the skin on other parts of the body behave in a very similar way. Very extensive studies have been performed on the friction between fingers and flat smooth and rough surfaces [27, 37]. Very high friction values have been observed during reciprocating sliding on smooth surfaces. This has been explained as resulting from an increase in the moisture content at the interface due to the high concentration of sweat glands on the fingers (and hands).

Theory shows that for the contact between elastic solids with randomly rough surfaces, the area of real contact A is proportional to the normal force F_N as long as the area of real contact is small compared to the nominal contact area A_0. If the friction force is assumed to be proportional to the area of real contact, the friction coefficient will be independent of the normal load (Coulombs friction law). Experiment for skin have shown that the friction coefficient is nearly independent of the load or nominal squeezing pressure [1]. The small deviation sometimes observed may be attributed to the complex nature of the skin which, e.g., exhibit spatially inhomogeneous (layered) viscoelastic properties. Viscoelasticity will also result in a contact area which depends on the sliding speed which will contribute to the (usually weak) velocity dependence of the friction coefficient. Thus, describing the exact load and velocity dependency of the skin friction would require information about the skin viscoelasticity properties not known at this time and we will not address this topic here.

The area of real contact we calculate is based on an accurate and well tested theory, and we have used measured or estimated elastoplastic properties of dry and wet skin, and the measures surface topography of the skin. Thus, we believe our estimation of the area of real contact is accurate. Earlier theoretical estimations of the area of real contact have not included the surface roughness on all length scales. The nominal contact pressures used in experimental friction studies of skin is usually very low (of order 10 kPa) compared to most other contact mechanics applications, which result in a small area of real contact in the range $A/A_0 \sim 10^{-3}$ (for wet skin) to $\sim 10^{-4}$ (for dry skin). We note that the area of real contact (as long as $A/A_0 \ll 1$) is determined by the elastoplastic properties of the top skin layer (stratum corneum) alone, and does not depend on the much softer underlying tissue (but the macroscopic deformations depends of course on the softer underlying tissue). For wet skin the stratum corneum has a similar elastic modulus as of rubber. For tires it has been shown that the area of real tire-road contact is only a few % of the nominal contact area [11]. In the present case, the contact area is a factor ~ 30 smaller but this mainly reflect the much lower nominal contact pressure (typically ~ 10 kPa for skin but ~ 300 kPa for tires).

Some results presented above may also be relevant for many other biological systems. Thus, hair, wool, nails, feather, hooves, horn and the outer layer of the skin (stratum corneum) involved in the study above, all have keratin (a fibrous protein with disulphide cross-links) as a major constituent. Thus, hair consists of approximately 97% of keratin. The surface of keratin contains negatively-charged amino acids and the natural hair-water-hair interface is (slightly) hydrophilic resulting (for drying hair) in the formation of water capillary bridges between hair fibers and bad combing properties. The "conditioners" used in hair care applications usually contains surfactants, which do not wash out completely, because their hydrophilic ends strongly bind to keratin. The hydrophobic ends of the surfactant molecules then act as the new hair surface making the hair-water-hair interface hydrophobic, which facilitate the removal of fiber entanglements during combing of weakly wet (during drying) hair. Just like for the top skin layer, hair can absorb a lot of water which changes its elastic and frictional properties.

Atmospheric water can be absorbed by biological materials of attachment devices of geckos and spiders. Higher water content in the vertebrate keratin and arthropod cuticle leads to the reduction of the elasticity modulus and to an increased flexibility of materials [38]. This results in higher adaptability of spatulae and setae to uneven surface profiles. This argument was recently used as an explanation for humidity-enhanced adhesion of gecko setae [39].

Finally, we note that fluid film lubrication of skin in water is promoted by surfactants that aid wetting, and also cause the the surfaces (e.g., glass and skin) to separate at asperity tips be electrical double-layer repulsion between charged adsorbed layers [35]. Thus, experiment have shown a strong reduction in the skin/glass friction in water if a surfactant is added to the water which form adsorbed layer on the skin with negative charged molecules. Since the glass surface is naturally negative charged a repulsive interaction will prevail between the surfaces. Double-layer repulsion is also likely the reason for the slippery or slimy feel of a mild aqueous caustic solution or dilute aqueous soap and detergent solution [35]. Similar effects have been observed for smooth rubber-glass contacts in water with surfactants which adsorb on the rubber surface [40]. In this case, the surfaces can be separated by fluid layers 10–30 nm thick under static loading conditions in the pressure range 10–60 kPa, and these films are maintained during sliding resulting in extremely low sliding friction coefficients.

8 Summary and Conclusion

We study the contact mechanics and friction for dry and lubricated human skin. The surface topography is studied using an optical method and the surface roughness power spectrum is obtained. The Persson contact mechanics theory is used to calculate the dependency of the contact area on the magnification for both dry and wet skin. For dry skin, plastic yielding becomes important and will determine the area of real contact at the highest magnification. The measured friction coefficient [M.J. Adams et al., Tribol Lett 26:239, 2007] on both dry and wet skin can be explained assuming

that a frictional shear stress $\sigma_f \approx 15$ MPa act in the area of real contact during sliding. This frictional shear stress is typical for sliding on polymer surfaces, and for thin (nanometer) confined fluid films. The big increase in the friction, which has been observed for glass sliding on wet skin as the skin dries up, can be explained as resulting from the increase in the contact area arising from the attraction of capillary bridges. This effect is predicted to operate as long as the water layer is thinner than ~ 14 μm, which is in good agreement with the time period (of order 100 s) over which the enhanced friction is observed (it takes about 100 s for ~ 14 μm water to evaporate at 50% relative humidity and at room temperature). We calculate the dependency of the sliding friction coefficient on the sliding speed on lubricated surfaces (Stribeck curve). We show that sliding of a sphere and of a cylinder gives very similar results if the radius and load on the sphere and cylinder are appropriately related. When applied to skin the calculated Stribeck curve is in good agreement with experiment, except that the curve is shifted by one velocity-decade to higher velocities than observed experimentally. We tentatively explain this by the role of the skin and underlying tissues viscoelasticity of the contact mechanics.

Appendix A: Capillary Adhesion; Role of Humidity

In Sect. 5, we studied the influence of relative thick water films (average film thickness of order $\sim 1-10$ μm) on the skin-glass contact mechanics. Such film thickness prevail, for example, during drying of an originally flooded contact. Similar film thickness may prevail during sweating. Here, we consider instead the skin in equilibrium with humid air as a function of the air relative humidity. For most humidity this implies water film thickness of order nanometers.

Figure 16 shows the logarithm (with 10 as basis) of the relative contact area as a function of the relative humidity. If the elastic modulus of the stratum corneum would take the same value as in the wet (or 100% relative humidity) state, $E_0 \approx 7$ MPa, for all relative humidity, then capillary adhesion for small relative humidity would be strong enough to bring the surfaces into nearly complete contact. However, in reality the elastic modulus rapidly increases with decreasing relative humidity (see Fig. 17), and the influence of the capillary adhesion for relative humidity below 90% is negligible. This is illustrated in Fig. 16 with a calculation with $E_0 = 70$ MPa, for which case the area of real contact is nearly independent of the relative humidity and determined by the applied load or pressure.
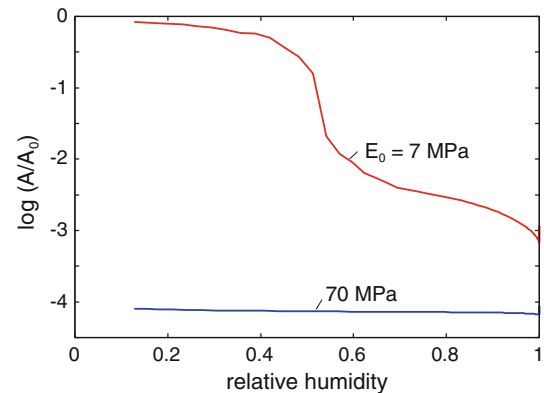
Fig. 16 The logarithm (with 10 as basis) of the relative contact area as a function of the relative humidity. If the elastic modulus of the stratum corneum would take its wet (or 100% relative humidity) value, $E_0 = 7$ MPa, for all relative humidity's, the capillary adhesion for small relative humidity would be strong enough to bring the surfaces into nearly complete contact. However, in reality the elastic modulus rapidly increases with decreasing relative humidity and the influence of the capillary adhesion for relative humidity below 90% is negligible. This is illustrated with a calculation with $E_0 = 70$ MPa for which case the area of real contact is nearly independent of the relative humidity and determined by the applied load or pressure. For the applied pressure $p_0 = 6.83$ kPa
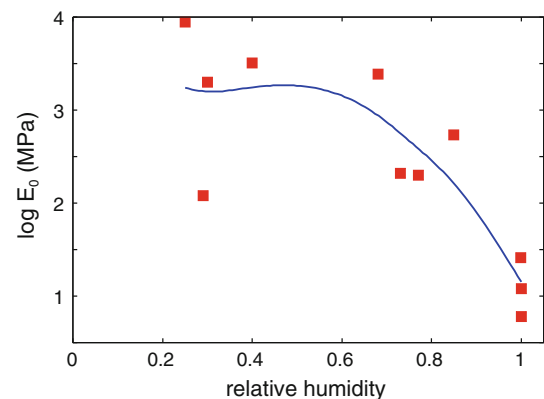
Fig. 17 The logarithm (with 10 as basis) of the Young's elastic modulus of the stratum corneum as a function of the relative humidity. The *blue line* is an approximate cubic spline fit to the experimental data. Based on experimental data obtained by Park and Baddiel, Papir, Koutroupi, Nikolopoulos, Gardner and Briggs and Yuan and Verma. Adopted from [41]

The calculation presented above (and in Ref. [15]) shows that if an elastic solid is soft enough, for a smooth hydrophilic interface there will be a strong increase in the contact area for some humidity range. This effect may be important in many situations, e.g., for rubber friction involving smooth hydrophilic interfaces, since the elastic modulus of rubber is nearly independent of the humidity and of similar magnitude as that of wet stratum corneum. This may contribute to the friction for, e.g., rubber wiper blades sliding on glass [17].

Appendix B: Mixed Lubrication; Approximate Mapping of Elliptic Contact on Cylinder Contact

In Sect. 6.1 we have shown how one can (approximately) map the sliding dynamics of a sphere on a lubricated substrate on a problem of a cylinder sliding on the same substrate, which is useful from a computational point of view, but also interesting from a conceptional point of view. This type of mapping should be even more accurately for a Hertz elliptic contact with the sliding direction orthogonal to the major elliptic axis (see Fig. 18).

We determine the radius of the cylinder and the load on the cylinder so that (a) the average Hertz contact pressure are the same, and (b) so that the condition $r_e = w\sqrt{(2/3)}$ is satisfied, where w is the width of the Hertz infinite rectangular contact strip for the cylinder, and r_e an effective radius of the elliptic contact region defined by:

$$\frac{1}{r_e^2} = \frac{1}{2}\left(\frac{1}{a^2} + \frac{1}{b^2}\right)$$

The latter condition guaranty the same fluid squeeze-out time for an infinite rectangular sheet (width w) as for an elliptic disk (with the major and minor axis a and b) (both rigid and with identical applied squeezing pressures). For the special case of a circular contact region, $a = b = r_0$ so that $r_e = r_0$ and the condition above reduces to $r_0 = w\sqrt{(2/3)}$ which was used in Sect. 6.1.

Assume that the interfacial separation $h(x, y)$ between the (undeformed) surfaces is of the form

$$h = \frac{x^2}{2R_1} + \frac{y^2}{2R_2}$$

We define the effective radius $R_e = (R_1 R_2)^{1/2}$. Thus for a sphere (radius R_s) in contact with the flat $R_1 = R_2 = R_s$ and $R_e = R_s$. The Hertz elliptic contact mechanics can be expressed using the complete elliptic integral of the first $K(x)$ and the second $E(x)$ kind, which are easy to evaluate using the integral representations

$$K(x) = \int_0^{\pi/2} d\phi \left(1 - x^2 \sin^2 \phi\right)^{-1/2},$$

and

$$E(x) = \int_0^{\pi/2} d\phi \left(1 - x^2 \sin^2 \phi\right)^{1/2}.$$

Defining

$$F_1^3 = \frac{4}{\pi e^2}\left(\frac{b}{a}\right)^{3/2}\left([(a/b)^2 E(e) - K(e)][K(e) - E(e)]\right)^{\frac{1}{2}}$$
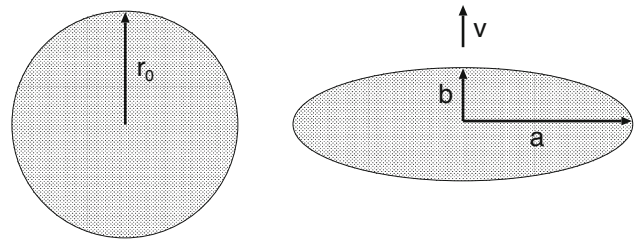
where

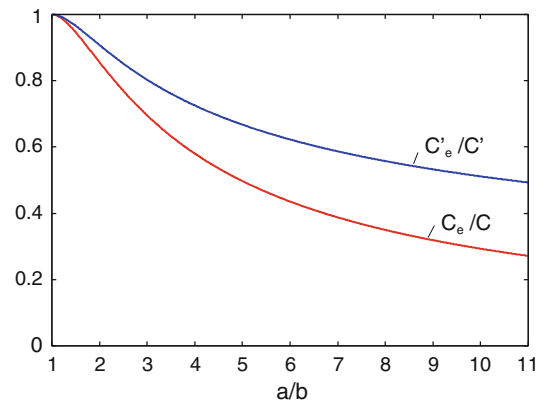Fig. 18 Hertz contact region for sphere on flat (left) and ellipse on flat (right)

Fig. 19 The factors C_e/C and C'_e/C' (where $C \approx 0.567$ and $C' \approx 0.429$) as a function of the ratio a/b between the ellipse major and minor axis

$$e = \left(1 - \frac{b^2}{a^2}\right)^{1/2}$$

we can write the average contact pressure $\bar{p}_e$ and the radius r_e as [31]

$$\bar{p}_e = \frac{2}{3\pi}\left(\frac{6F_N E^{*2}}{R_e^2}\right)^{1/3} F_1^{-2}, \quad r_e = \left(\frac{3F_N R_e}{4E^*}\right)^{1/3} G_1$$

where

$$G_1 = F_1\left[\frac{1}{2}\left(\frac{b}{a} + \frac{a}{b}\right)\right]^{-1/2}$$

Thus, we get

$$R_c = C_e R_e, \quad f_N = C'_e\left(\frac{E^* F_N^2}{R_e}\right)^{1/3} \tag{B1}$$

where

$$C_e = C F_1^3\left[\frac{1}{2}\left(\frac{b}{a} + \frac{a}{b}\right)\right]^{-1/2}$$

$$C'_e = C' F_1^{-1}\left[\frac{1}{2}\left(\frac{b}{a} + \frac{a}{b}\right)\right]^{-1/2}$$

In Fig. 19, we show C_e/C and C'_e/C' as a function of a/b.

Appendix C: Stribeck Curve for Skin; Role of Shear Thinning and Flow Factors

In Sect. 6.2, we have calculated the Stribeck curve for a hard sphere sliding on lubricated skin and compared to experiments where the skin where lubricated with silicon oil of different viscosity's. The calculated Stribeck curve is similar to the measured one but shifted by a factor ~ 20 to higher sliding velocity than observed. We have presented a tentative explanation for this related to the viscoelastic nature of the human skin and underlying tissues. In this section, we show that the deviation between experiment and theory cannot be attributed to inaccuracy in the fluid flow factors or shear thinning of the silicon oil since both effects gives very small changes in the Stribeck curve. We attribute this insensitivity of the Stribeck curve to the flow factors and shear thinning to the small contact pressure and large (average) interfacial separation even in the boundary lubrication region.

The fluid flow at the interface between solids with surface roughness is a very complex problem. However, if the surface roughness gradient is not too large one may average the basic equations of fluid flow over the surface roughness and obtain effective equations for smooth surfaces. In the effective equations enters the pressure and shear flow factors ϕ_p and ϕ_s which depends on the (average) local interfacial separation $\bar{u}$. For smooth surfaces $\phi_p = 1$ and $\phi_s = 0$ which we refer to as trivial pressure and shear flow factors. Similarly in the expression for the frictional shear stress enters three frictional shear stress factors ϕ_f, ϕ_{fs} and ϕ_{fp} which are also functions of $\bar{u}$. For smooth surfaces $\phi_f = \phi_{fp} = 1$, and $\phi_{fs} = 0$, which we refer to as trivial friction factors. In Ref. [29] one of us have shown how all these functions can be calculated in an approximate but accurate way, and we used this theory in the numerical calculations of the Stribeck curve presented in this article.

Figure 20 shows the calculated Stribeck curve including all fluid flow and frictional shear stress factors (red curve), and for trivial fluid flow and frictional shear stress factors (blue curve). There is negligible difference between the two curves and we conclude that an accurate knowledge of the fluid flow and frictional shear stress factors is not necessary for the present problem due to the large average separation between the surfaces.
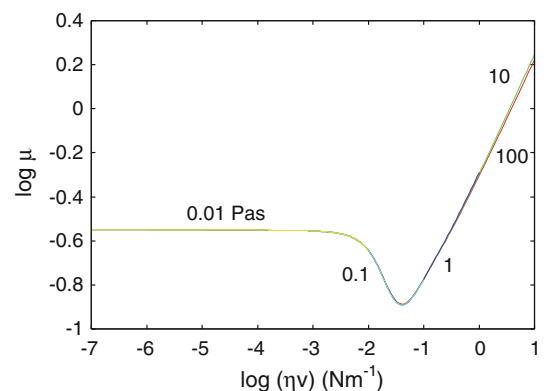
Figure 21 shows the calculated Stribeck curve for fluids with the (low-shear rate) viscosity's $\eta_0 = 0.01$, $0.1, \ldots, 100$ Pas including shear thinning. The shear thinning is described by using the effective viscosity [29, 33, 34]

$$\eta = \frac{\eta_0}{1 + (\eta_0/B)\dot{\gamma}^n}$$

where (using SI units) $B = 10^4$ and $n = 0.8$. The shear rate $\dot{\gamma} = v/u$ (where u is the film thickness). This expression for the
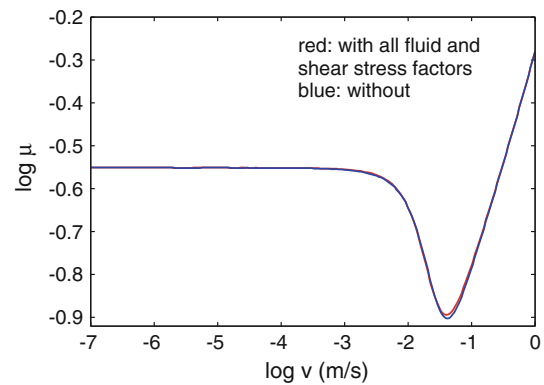
Fig. 20 The *red line* is the calculated Stribeck curve including all fluid flow and frictional shear stress factors, while the *blue line* is with trivial fluid flow and frictional shear stress factors. For the fluid viscosity $\eta = 1$ Pa s. See text for details (Color figure online)

Fig. 21 The calculated Stribeck curve for fluids with viscosities $0.01, 0.1, \ldots, 100$ Pa s including shear thinning. See text for details

effective viscosity describes accurately the shear thinning of silicon oils of different viscosity's [33, 34]. Not that shear thinning start at lower shear rate as the low-shear rate viscosity η_0 increases. Thus, shear thinning becomes important when $\dot{\gamma} > \dot{\gamma}_c = (B/\eta_0)^{1/n}$. For example, for $\eta_0 = 1$ Pa s shear thinning start when $\dot{\gamma} > \dot{\gamma}_c \approx 10^5 \, \text{s}^{-1}$. Note that including shear thinning has a negligible influence on the Stribeck curve. This is again due to the low contact pressure and large average interfacial separation in the present case.

References

1. Adams, M.J., Briscoe, B.J., Johnson, S.A.: Friction and lubrication of human skin. Tribol. Lett. **26**, 239–253 (2007)
2. Park, A.C., Baddiel, C.B.: Effect of saturated salt solutions on elastic properties of stratum corneum. J. Soc. Cosmet. Chem. **23**, 3, 471–479 (1972)
3. Warman, P.H., Ennos, A.R.: Fingerprints are unlikely to increase the friction of primate fingerpads. J. Exp. Biol. **212**, 2016–2022 (2009)

4. Derler, S., Gerhardt, L.-C.: Tribology of skin: review and analysis of experimental results for the friction coefficient of human skin. Tribol. Lett. **45**, 1–27 (2012)

5. Persson, B.N.J.: Contact mechanics for randomly rough surfaces. Surf. Sci. Rep. **61**, 201–227 (2006)

6. Persson, B.N.J., Albohr, O., Tartaglino, U., Volokitin A.I., Tosatti, E.: On the nature of surface roughness with application to contact mechanics, sealing, rubber friction and adhesion, J. Phys.: Condens. Matter 17, R1–R62 (2005)

7. Kendall, M.A.F., Carter, F.V., Mitchell, T.J., Bellhouse, B.J.: University of Oxfort, UK, research article: *Comparison of the transdermal ballistic delivery of micro-particles into the human and porcine skin.* http://www.dtic.mil/dtic/tr/fulltext/u2/a410062.pdf

8. Persson, B.N.J., Ganser, C., Schmied, F., Teichert, C., Schennach, R., Gilli, E., Hirn, U.: Adhesion of cellulose fibers in paper, subm. to J. Phys.: Condens. Matter

9. Persson, B.N.J.: Theory of rubber friction and contact mechanics. J. Chem. Phys. **115**, 3840–3861 (2001)

10. O'Sullivan, T.C., King, R.B.: Sliding contact stress-field due to a spherical indenter on a layered elastic half-space. ASME J. Tribol. **110**, 235–240 (1988)

11. Persson, B.N.J.: Contact mechanics for layered materials with randomly rough surfaces. J. Phys.: Condens. Matter **24**, 095008 (2012)

12. Carbone, G., Lorenz, B., Persson, B.N.J., Wohlers, A.: Contact mechanics and rubber friction for randomly rough surfaces with anisotropic statistical properties. Eur. Phys. J. E. **29**, 275–284 (2009)

13. Sivebaek, I.M., Samoilov, V.N., Persson, B.N.J.: Frictional properties of confined polymers. Eur. Phys. J. E. **27**, 37–46 (2008)

14. Sivebaek, I.M., Samoilov, V.N., Persson, B.N.J.: Effective viscosity of confined hydrocarbons. Phys. Rev. Lett. **108**, 036102 (2012)

15. Persson, B.N.J.: Capillary adhesion between elastic solids with randomly rough surfaces. J. Phys.: Condens. Matter **20**, 315007 (2008)

16. Persson, B.N.J., Volokitin, A.I., Tosatti, E.: Role of the external pressure on the dewetting of soft interfaces. Eur. Phys. J. E. **11**, 409–413 (2003)

17. Deleau, F., Mazuyer, D., Koenen, A.: Sliding friction at elastomer/glass contact: influence of the wetting conditions and instability analysis. Tribol. Int. **42**, 149–159 (2009)

18. Wangenheim, M., Kröger, M.: Friction phenomena on microscale in technical contacts with rubber. Proceedings 9th ASME Conference on Engineering Systems Design and Analysis 3, ESDA (2008), Haifa, Israel. S., pp. 541–547

19. Homann, H.: Haften Spinnen an einer Wasserhaut. Naturwissenschaften **44**, 318–319 (1957). doi:10.1007/BF00630926

20. Huber, G., Mantz, H., Spolenak, R., Mecke, K., Jacobs, K., Gorb, S.N., Arzt, E.: Evidence for capillarity contributions to gecko adhesion from single spatula nanomechanical measurements. Proc. Natl Acad. Sci. USA **102**, 16293–16296 (2005). doi:10.1073/pnas.0506328102

21. Niewiarowski, P.H., Lopez, S., Ge, L., Hagan, E., Dhinojwala, A.: Sticky gecko feet: the role of temperature and humidity. PLoS ONE **3**, e2192 (2008). doi:10.1371/journal.pone.0002192

22. Wolff, J.O., Gorb, S.N.: The influence of humidity on the attachment ability of the spider Philodromus dispar (Araneae, Philodromidae). Proc. R. Soc. B **279**, 139–143 (2012). doi:10.1098/rspb.2011.0505

23. Gerhardt, L.-C., Strssle, V., Lenz, A., Spencer, N.D., Derler, S.: Influence of epidermal hydration on the friction of human skin against textiles. J. R. Soc. Interface **5**, 1317–1328 (2008)

24. Hendriks, C., Franklin, S.: Influence of surface roughness, material and climate conditions on the friction of human skin. Tribol. Lett. **37**, 361–373 (2010)

25. Kwiatkowska, M., Franklin, S.E., Hendriks, C.P., Kwiatkowski, K.: Friction and deformation behaviour of human skin. Wear **267**, 1264–1273 (2009)

26. Tomlinson, S.E., Lewis, R., Liu, X., Texier, C., Carr, M.J.: Understanding the friction mechanisms between the human finger and flat contacting surfaces in moist conditions. Tribol. Lett. **41**, 283–294 (2011)

27. Pasumarty, S.M., Johnson, S.A., Watson, S.A., Adams, M.J.: Friction of the human finger pad: influence of moisture, occlusion and velocity. Tribol. Lett. **44**, 117–137 (2011)

28. Persson, B.N.J., Scaraggi, M.: On the transition from boundary lubrication to hydrodynamic lubrication in soft contacts. J. Phys.: Condens. Matter **21**, 185002 (2009)

29. Persson, B.N.J., Scaraggi, M.: Lubricated sliding dynamics: flow factors and Stribeck curve. Eur. Phys. J. E **34**, 113 (2011)

30. Scaraggi, M., Carbone, G., Persson, B.N.J., Dini, D.: Lubrication in soft rough contacts: a novel homogenized approach. Part I—theory. Soft Matter **7**, 10395–10406 (2011)

31. Johnson, K.L.: Contact Mechanics, p. 452. Cambridge University Press, Cambridge (1966)

32. Bowen, J., Cheneler, D., Andrews, J.W., Avery, A.R., Zhand, Z., Ward, M.C.L., Adams, M.J.: Application of colloid probe atomic force microscopy to the adhesion of thin films of viscous and viscoelastic silicone fluids. Langmuir **27**, 11489–11500 (2011)

33. Stephens, T.S., Winter, H.H., Gottlieb, M.: The steady shear viscosity of filled polymeric liquids described by a linear superposition of 2 relaxation mechanisms. Rheol. Acta **27**, 263–272 (1988)

34. http://www.clearcoproducts.com/silicones_library.html

35. Johnson, S.A., Gorman, D.M., Adams, M.J., Briscoe, B.J.: The friction and lubrication of human stratum corneum. In: D. Dowson et al (eds.) Thin films in technology, pp 663–672. Elsevier Science Publishers (1993)

36. Persson, B.N.J.: Rolling friction for hard cylinder and sphere on viscoelastic solid. Eur. Phys. J. E. **33**, 327–333 (2010)

37. Tomlinson, S.E., Lewis, R., Carre, M.J.: The effect of normal force and roughness on friction in human finger contact. Wear **267**, 1311–1318 (2009)

38. Vincent, J.F., Wegst, U.K.: Design and mechanical properties of insect cuticle. Arthr. Str. Dev. **33**, 187–199 (2004). doi:10.1016/j.asd.2004.05.006

39. Puthoff, J.B., Prowse, M.S., Wilkinson, M., Autumn, K.: Changes in materials properties explain the effects of humidity on gecko adhesion. J. Exp. Biol. **213**, 3699–3704 (2010). doi:10.1242/jeb.047654

40. Richards, S.C., Roberts, A.D.: Boundary lubrication of rubber by aqueous surfactant. J. Phys. D **25**, A76–A80 (1992)

41. Geerligs, M.: A literature review of the mechanical behaviour of the stratum corneum, the living epidermis and the subcutaneous fat tissue, Technical Note PR-TN 2006/00450, Koninklijke Philips Electronics N.V. (2006)